Three-dimensional structure extraction and evaluation of microvessels in cardiac tissue imaged via confocal microscopy

Shotaro Kaneko[1], Yuichiro Arima[2], Masahiro Migita[3], and Masashi Toda[3]

[1] Graduate School of Science and Technology, Kumamoto University, Kumamoto 860-8555, Japan
[2] Dept. of Cardiovascular Medicine, Kumamoto University, Kumamoto 860-0811, Japan
[3] Center for Management of Information Technologies, Kumamoto University, Kumamoto 860-8555, Japan
228d8710@st.kumamoto-u.ac.jp

Abstract. Because cardiac disease accounts for 15% of all deaths in Japan, there is an urgent need to elucidate its pathogenesis and establish new treatment methods. However, the mechanisms underlying the pathogenesis of cardiac disease are still unclear. With the advancement of computer technology in recent years, elucidation of the pathophysiology at the cellular level in the heart is expected. Many previous studies investigated myocardial tissues, which is a three-dimensional body, in two dimensions. Therefore, in this study, we propose 'vascular straightness' and 'angle between cardiomyocyte nucleus and vascular skeleton', which quantitatively evaluate the vascular structure and the relationship between cardiomyocytes and blood vessels, respectively, by performing three-dimensional analysis of microscopic images of myocardial tissues of mice. We calculated the proposed indices in wild-type (WT) and knockout (KO) mice and confirmed the differences. In the future, we intend to test for significant differences using statistical analysis, propose indices for the quantitative evaluation of the vessel thickness and surface structure, and classify mice into healthy mice and mice with heart defects based on the proposed indices.

Keywords: Three-dimensional medical imaging, cardiac disease, microvascular.

1 Introduction

Heart disease accounts for 15% of all deaths in Japan, second only to malignant neoplasms (tumours), and the mortality rate is increasing every year [1]. Heart failure accounts for approximately half of all deaths owing to heart disease [1]. Although drug therapy for heart failure has made steady progress compared to the past, it is often ineffective for severe cases of heart failure, and no established treatment other than heart transplantation is currently available [2]. Heart transplantation has been initiated in Japan. However, the number of donors is significantly fewer than that required for transplantation, and it is difficult to imagine that this treatment will be-

come widely available in the future [2]. Therefore, there is an urgent need to elucidate the pathogenesis of heart failure and establish new treatment methods.

With the development of computer technology, the pathophysiology of heart failure is expected to be clarified at the cellular level. Myocardial cells, the main constituents of the heart, have been used to reveal the pathophysiology of heart failure. However, because it is difficult to use human cardiomyocytes, studies using cardiomyocytes from mice, which are also mammals, have been conducted. A representative study reported the cross-sectional area of cell nuclei from myocyte images of mouse cardiomyocytes captured using a microscope under conditions similar to heart failure [3]. However, most studies investigated cardiomyocytes, which are three-dimensional bodies, in two dimensions. Therefore, additional information might be obtained by conducting three-dimensional analysis of tiny cells, such as cardiomyocytes. In addition, because cardiomyocytes and other cells coexist in the heart, it is desirable to classify nucleated cells and analyse their volume and positional relationships as three-dimensional information. Single-cell analysis [4] has revealed the mechanism of cardiomyocyte hypertrophy and failure by machine learning. However, single-cell analysis is expensive and time-consuming, as it isolates cells and focuses on a single cell. In addition, because the cells are isolated, it is impossible to obtain information on their original shape and positional relationship when they exist as cardiac tissues. A representative three-dimensional analysis of nuclei was performed by Alexandr et al. [5]. In their study, modelling, analysis, and classification of cell nuclei and nucleoli were performed in three dimensions. They compared the morphology of serum-starved and proliferating fibroblasts, followed by a comparison of epithelial and mesenchymal human prostate cancer cell lines to classify fibroblasts, and epithelial and mesenchymal cells, respectively. However, the myocardium was not investigated, and only morphological information (for example, volume and surface area) of cell nuclei and nucleoli was utilised.

In this study, we examined a method for three-dimensional image analysis of cellular tissues of the myocardial region. Fig. 1 shows a myocardial tissue microscopy image of the mouse used in this study. The contributions of this study are as follows:

- Regions complemented by missing holes in endothelial cell membrane images were extracted, in which no contrast agent was used, and the areas inside blood vessels and where endothelial cell nuclei exist are not fluorescent.
- To quantitatively evaluate the structure of blood vessels and the relationship between cardiomyocytes and blood vessels, we proposed two indices: “straightness of blood vessels” and “angle between the cardiomyocyte nuclei and blood vessels.”
- We calculated the index values of the proposed method in wild-type (WT) and knockout (KO) mice and confirmed the difference between the two.

2 Method

2.1 Extraction of vascular regions

Fig. 2(a) shows a stained image of a vascular endothelial cell membrane. This image was smoothed using an anisotropic diffusion filter [6, 7] (Fig. 2(b)). The Otsu method [8], a widely used binarisation method, does not successfully extract the vascular endothelial region because of differences in the fluorescent intensity values for different locations, even in the vascular endothelial cell membrane. Therefore, adaptive thresholding [9] was used in this study (Fig. 2(c)). Fig. 2(d) shows the endothelial region image after noise removal and other processing steps for the binarised image. The endothelial cell nuclei and interior of the vessels were not stained, resulting in the appearance of missing holes (Fig. 3(a),(b)). This explains why the centre line cannot be captured satisfactorily when skeletonisation is performed, as described below. Therefore, it is necessary to fill these closed regions. Filling in the closed regions is performed in the xy-, yz-, and zx-planes. If the edges or vertices of a pixel touch, the pixel is connected [10]. Figs. 2(e) and 3(c) show the endothelial region after filling the closed region.

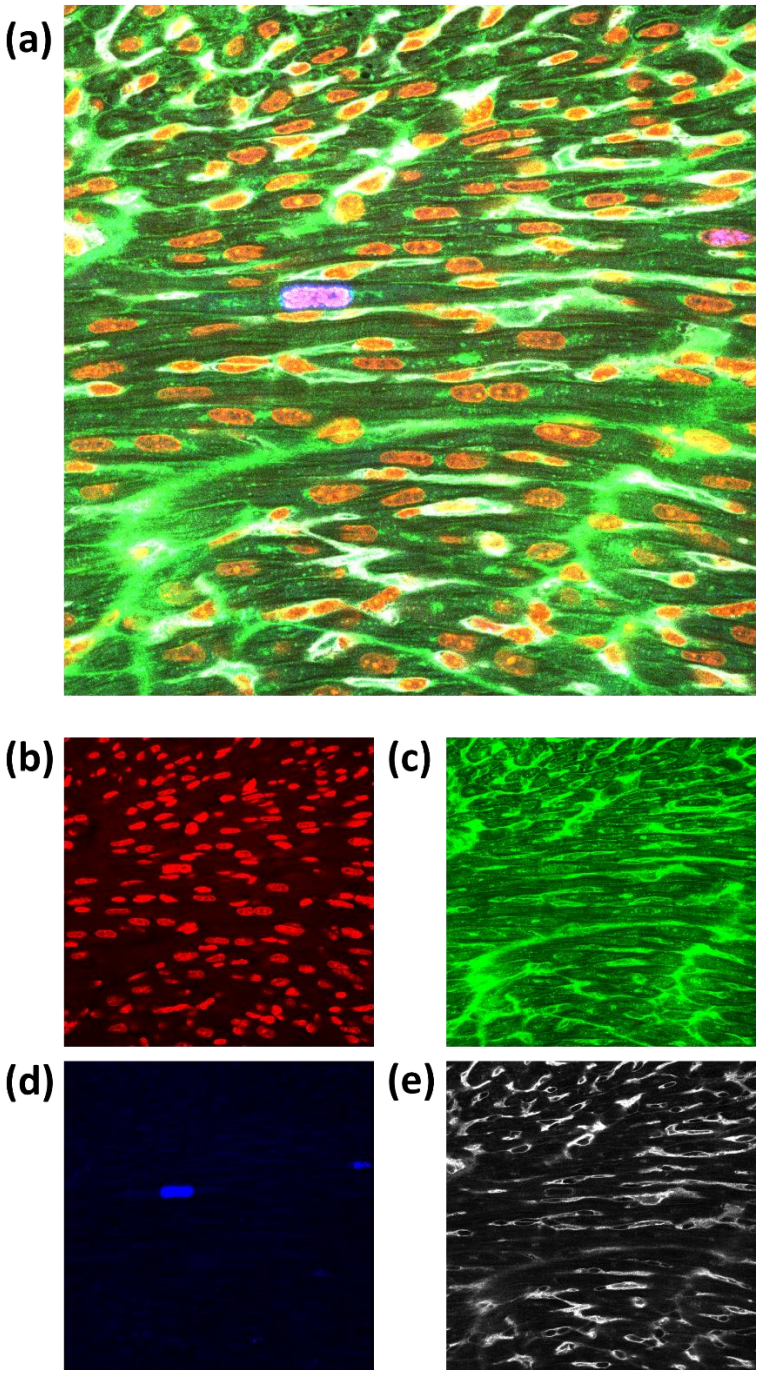

Fig. 1. (a) Myocardial tissue microscopic image. (b) Cell nucleus. (c) Cell membrane. (d) Dividing cell nucleus. (e) Vascular endothelial cell membrane.

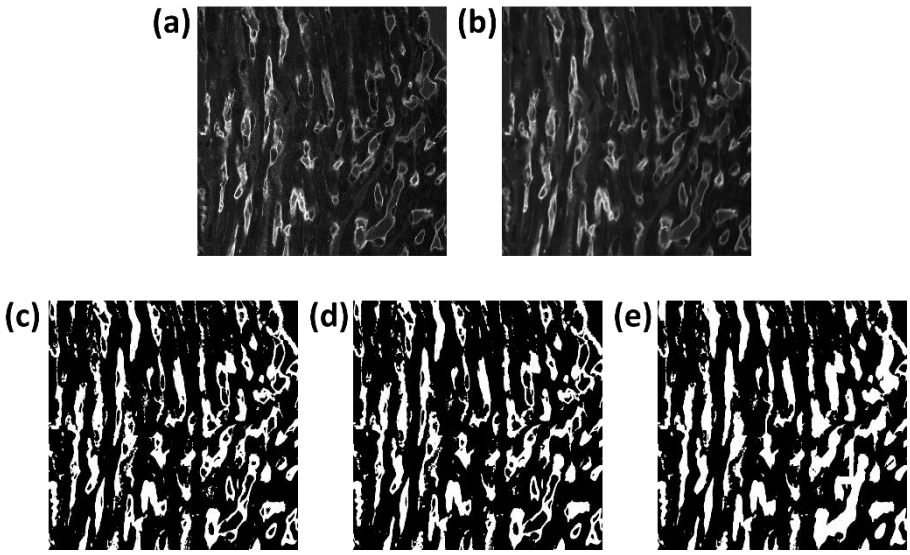

Fig. 2. (a) Vascular endothelial cell membrane. (b) Membrane smoothed with anisotropic diffusion filter. (c) Binarisation with adaptive thresholding. (d) Vascular endothelial area after noise removal and other processes. (e) Vascular endothelial area after hole filling.

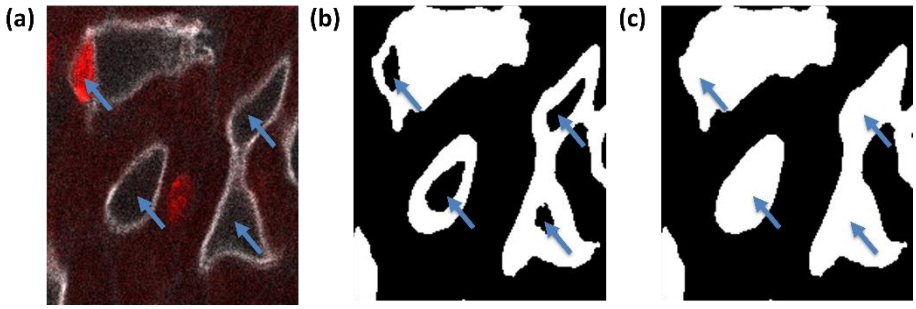

Fig. 3. (a) Cell nuclei (red) and vascular endothelial cell membrane (white). (b) Vascular endothelial area before hole filling. (c) Vascular area after hole filling.

2.2 Blood vessel region skeletonisation and bifurcation point extraction

Skeletonisation [11, 12], a method for determining the centreline of a vessel, was performed on the endothelial region of a vessel after hole filling, extracted in the previous section, to obtain the basic structure of the vessel.

After skeletonisation of the vascular region, branching points of the skeleton were identified. A bifurcation point is a voxel where multiple branches intersect [13, 14]. Fig. 4 shows the extracted vessel region (grey), the vessel skeleton (magenta), and the bifurcation point (cyan). In addition, a single-vessel skeleton is defined here as the end between or from branch points (Fig. 5).

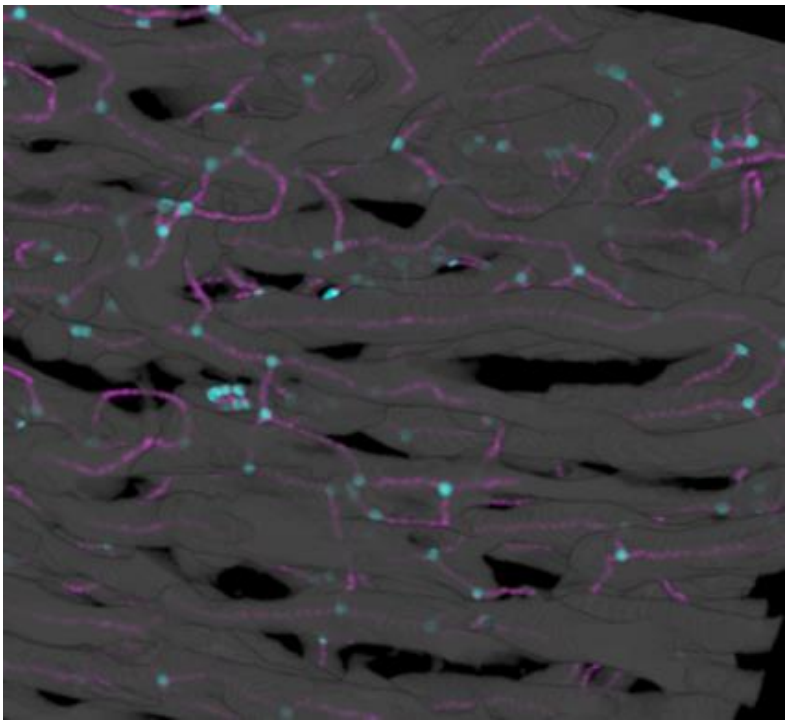

Fig. 4. Extracted blood vessel regions (grey), blood vessel skeleton (magenta), and bifurcation points (cyan).

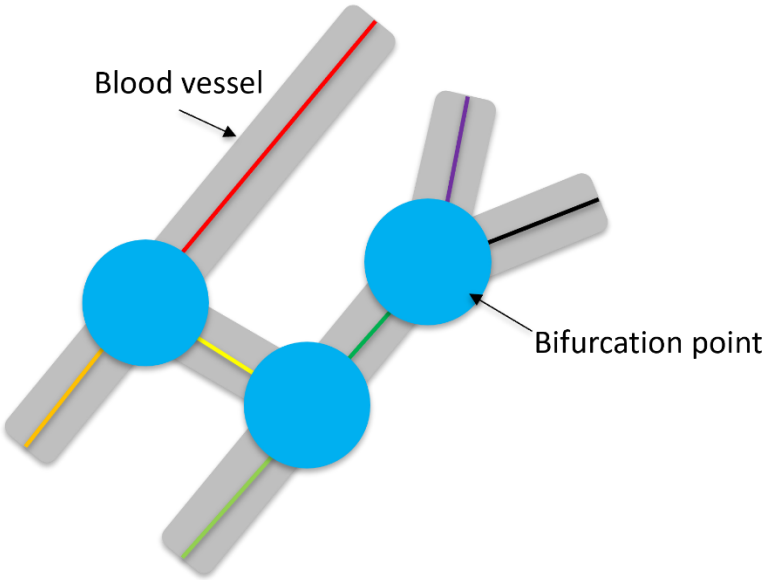

Fig. 5. Diagram of single-blood vessel skeleton. In this figure, there are seven vessel skeletons.

2.3 Cell Nucleus Classification

The myocardial tissue microscopic images used in this study contained vascular endothelial cells, smooth muscle cells, fibroblasts, and other cells, in addition to myocardial cells. Therefore, it is necessary to classify cells by type and identify the cardiomyocytes to analyse the relationship between cardiomyocytes and blood vessels. Currently, it is difficult to extract cellular regions from stained images of cell membranes; therefore, analysis is conducted on cell nuclei, from which it is relatively easy to extract regions. To classify cell nuclei, we utilised a method for identifying vascular endothelial cells from myocardial tissue microscopy images of mice [15]. This method classifies cell nuclei into vascular endothelial cell nuclei and other types of cell nuclei based on the 'coverage ratio', which quantitatively expresses how much of the cell nucleus is covered by the vascular endothelial area, and can classify the nuclei into vascular endothelial cell nuclei and other types with approximately 85% accuracy. Vascular endothelial cell nuclei are covered by the vascular endothelium, whereas cardiomyocyte nuclei are not covered by vascular endothelium. Based on these characteristics, this study classified cardiomyocyte nuclei into three clusters: vascular endothelial cell nuclei with high coverage, cardiomyocyte nuclei with low coverage, and other cell nuclei.

2.4 Quantitative index for evaluating three-dimensional vascular structure

Vascular straightness

We propose 'straightness of blood vessels' as an index to quantitatively evaluate the three-dimensional structure of blood vessels. The straightness is calculated as follows:

$$s = \frac{d}{L} \tag{1}$$

where d is the Euclidean distance between the two ends of the vessel skeleton, and L is the length of the vessel skeleton.

Therefore, the closer the straightness value is to 1, the straighter the vessel.

Angles between myocardial cell nuclei and vascular skeleton

We propose the 'angle between the cardiomyocyte nucleus and vascular skeleton' as a quantitative measure of the relationship between cardiomyocytes and blood vessels. First, the long-axis direction of the cardiomyocyte nucleus was determined. In this study, principal component analysis [16] was used for a group of voxels constituting the myocardial cell nucleus, and the first principal component derived was used as the long-axis vector.

Next, the orientation of the vessel skeleton was determined. The two ends of the voxels comprising a single-vessel skeleton were determined, and the vector between these two points was considered the vector of the vessel skeleton.

Finally, the vessel skeleton corresponding to an individual myocyte nucleus and the angle between the vectors were determined. In the case of myocardial cell nuclei and blood vessels that are significantly far apart, it is difficult to assume that they interact.

In addition, it has been difficult to accurately extract cellular regions from cell membrane images, and the analysis is currently performed using myocardial cell nuclei. Therefore, we defined a region corresponding to each myocardial cell nucleus and focused only on blood vessels within that region. To determine the region corresponding to each myocyte nucleus, we used a three-dimensional Voronoi partition [17] with respect to the centre of gravity of all myocyte nuclei. Because the skeleton is similar to a line passing through the approximate centre of a blood vessel, many cardiomyocyte nuclei have no blood vessels within the three-dimensional Voronoi region when the inside−outside region was determined for the vessel skeleton. Because it is physiologically unlikely that no blood vessels correspond to a cardiomyocyte nucleus, an in/out judgement was performed on the surfaces of the blood vessels. Edge detection [18] was used to assess the vessel surface. For each vessel surface voxel, we assigned a labelling number corresponding to the labelling number of the vessel skeleton at the closest distance. The angles between the long-axis direction of the myocardial cell nucleus and the labelling number of the vessel surface within the three-dimensional Voronoi region and the corresponding vessel skeleton were then calculated. The angle is obtained by [19] as follows:

$$\theta = \cos^{-1}\frac{a \cdot b}{|a||b|} \tag{2}$$

where a is the direction of the long axis of the cardiomyocyte nucleus, b is the direction of the vascular skeleton, and $0° \leq \theta \leq 90°$. Fig. 6 shows an example of a cardiomyocyte nucleus and the corresponding blood vessel. The cardiomyocyte nucleus is represented by magenta, the direction of the long axis of the cardiomyocyte nucleus by a black arrow, the three-dimensional Voronoi region by green, the surfaces of the blood vessels within that region by red, and the surface of blood vessels outside the region by blue.

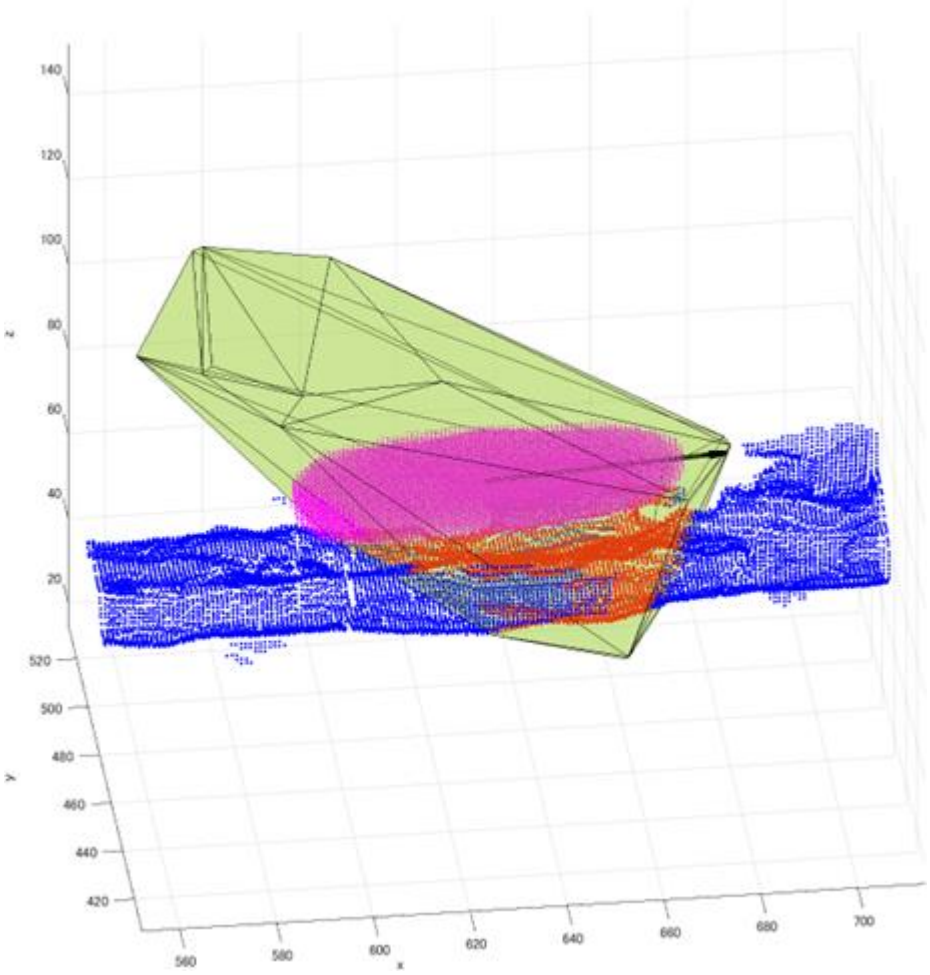

Fig. 6. Examples of myocardial cell nuclei and corresponding blood vessels.

3 Experiment

Table 1 lists the equipment and development environment used in the experiment. In this study, microscopic images of the hearts of neonatal mice were analysed. Microscopic images of cell nuclei, cell membranes, dividing cell nuclei, and vascular endothelial cell membranes were captured, each with fluorescence.

The experiment was performed using myocardial images of WT (normal) and KO mice of the same number of postnatal days. The KO mice were genetically modified to prevent them from producing HMG-CoA Synthase 2, an enzyme essential for synthesising ketone bodies, so that ketones are unavailable, and metabolism is affected [20]. The samples were three WT mice and three KO mice. Three images were captured from different parts of each individual.

The images of cell nuclei and vascular endothelial cells were fluorescent. Table 2 lists the details of the datasets. In this experiment, the straightness of the blood vessel and the angle between the myocardial cell nucleus and vascular skeleton were obtained using the proposed method for the dataset. The analysis was performed for blood vessel skeletons with lengths of 50–99 pixels (9.0188–17.8571 microns) and more than 100 pixels (18.0375 microns).

Table 1. Equipment and development environment

OS	MS Windows 10
CPU	i7-8700K (3.70 GHz)
RAM	40.0 GB
Development environment	MATLAB R2020b

Table 2. Details of dataset

Format	TIFF
Resolution (Width × Height × Depth)	1,024 × 1,024 × 169 (However, the depth of 221107_WT06_01 is 139.)
1 voxel (Width × Height × Depth)	0.1803752 × 0.1803752 × 0.2985004 (microns)
Colour type	Grayscale
Target	Neonatal murine
Shooting location	Myocardial tissue of the left atrium
Shooting object	Cell nucleus, cell membrane, dividing cell nucleus, and vascular endothelial cell membrane
Shooting equipment	Confocal laser scanning microscopy

4 Results

4.1 Results of cell nucleus classification

Table 3 lists the classification values of cell nuclei into three clusters based on coverage: vascular endothelial cell nuclei, myocardial cell nuclei, and other cell nuclei.

Table 3. Results of cell nucleus classification

Sample name	Vascular endothelial cell nuclei	Myocardial cell nuclei	Other cell nuclei	Total
221107_WT04_01	951 (35.0%)	1,176 (43.2%)	593 (21.8%)	2, 720
221107_WT04_02	855 (30.7%)	1,417 (50.9%)	511 (18.4%)	2,783
221107_WT04_03	833 (23.5%)	2,150 (60.7%)	557 (15.7%)	3,540
221107_WT06_01	757 (40.6%)	784 (42.1%)	323 (17.3%)	1,864
221107_WT06_02	748 (32.8%)	1,068 (46.8%)	464 (20.4%)	2,280
221107_WT06_03	665 (32.2%)	1,064 (51.6%)	334 (16.2%)	2,063
221117_WT7_01	715 (40.1%)	825 (46.2%)	244 (13.7%)	1,784
221117_WT7_02	721 (33.2%)	918 (42.3%)	530 (24.4%)	2,169
221117_WT7_03	613 (34.3%)	816 (45.7%)	358 (20.0%)	1,787
221107_KO2_01	845 (36.8%)	1,055 (46.0%)	395 (17.2%)	2,295
221107_KO2_02	945 (41.8%)	968 (42.8%)	347 (15.4%)	2,260
221107_KO2_03	722 (48.1%)	647 (43.1%)	131 (8.7%)	1,500
221107_KO05_01	637 (35.5%)	840 (46.8%)	319 (17.8%)	1,796
221107_KO05_02	757 (38.2%)	847 (42.8%)	377 (19.0%)	1,981
221107_KO05_03	519 (33.9%)	720 (47.0%)	294 (19.2%)	1,533
221117_KO2_01	789 (43.5%)	789 (43.5%)	234 (12.9%)	1,812
221117_KO2_02	650 (33.8%)	979 (50.9%)	296 (15.4%)	1,925
221117_KO2_03	638 (33.5%)	781 (41.0%)	487 (25.6%)	1,906

4.2 Results for blood vessel straightness and angle between myocardial cell nucleus and blood vessels

Fig. 7 shows the results for the straightness of the vessels, and Fig. 8. shows the values of the angle between the myocardial cell nucleus and vascular skeleton. Regarding the accuracy of the vascular area extraction, skeletonisation, and bifurcation point extraction, we had an expert examine at some of the data, who confirmed that there were no problems. The straightness visualisation shown in Fig. 9 indicates that the closer the straightness value is to 1, the straighter the blood vessel structure. We compared the differences in the proposed quantitative index between the WT and KO mice and found that both the straightness of blood vessels and the angle between the myocardial cell nuclei and blood vessels differed between samples obtained at different locations in the same individual as well as between individuals. This is attributed to the fact that some images showed blood vessels extending along the z-axis, whereas others showed vessels extending in the xy-plane. Moreover, the direction of the blood vessels is not constant, depending on the area being photographed.

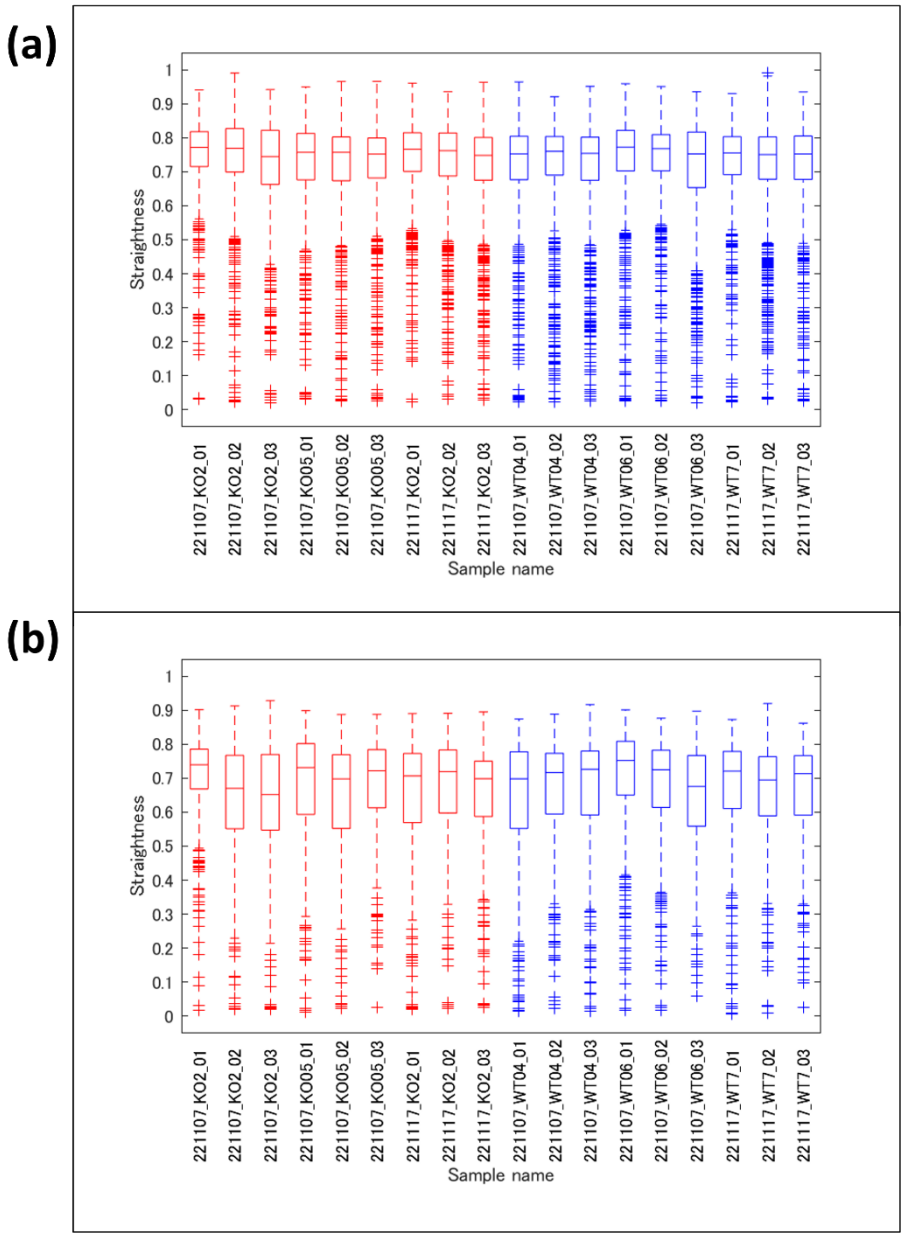

Fig. 7. Vascular straightness. (a) Vascular skeleton length of 50−99 pixels (9.0188− 17.8571 microns). (b) Vessel skeleton length exceeding 100 pixels (18.0375 microns).

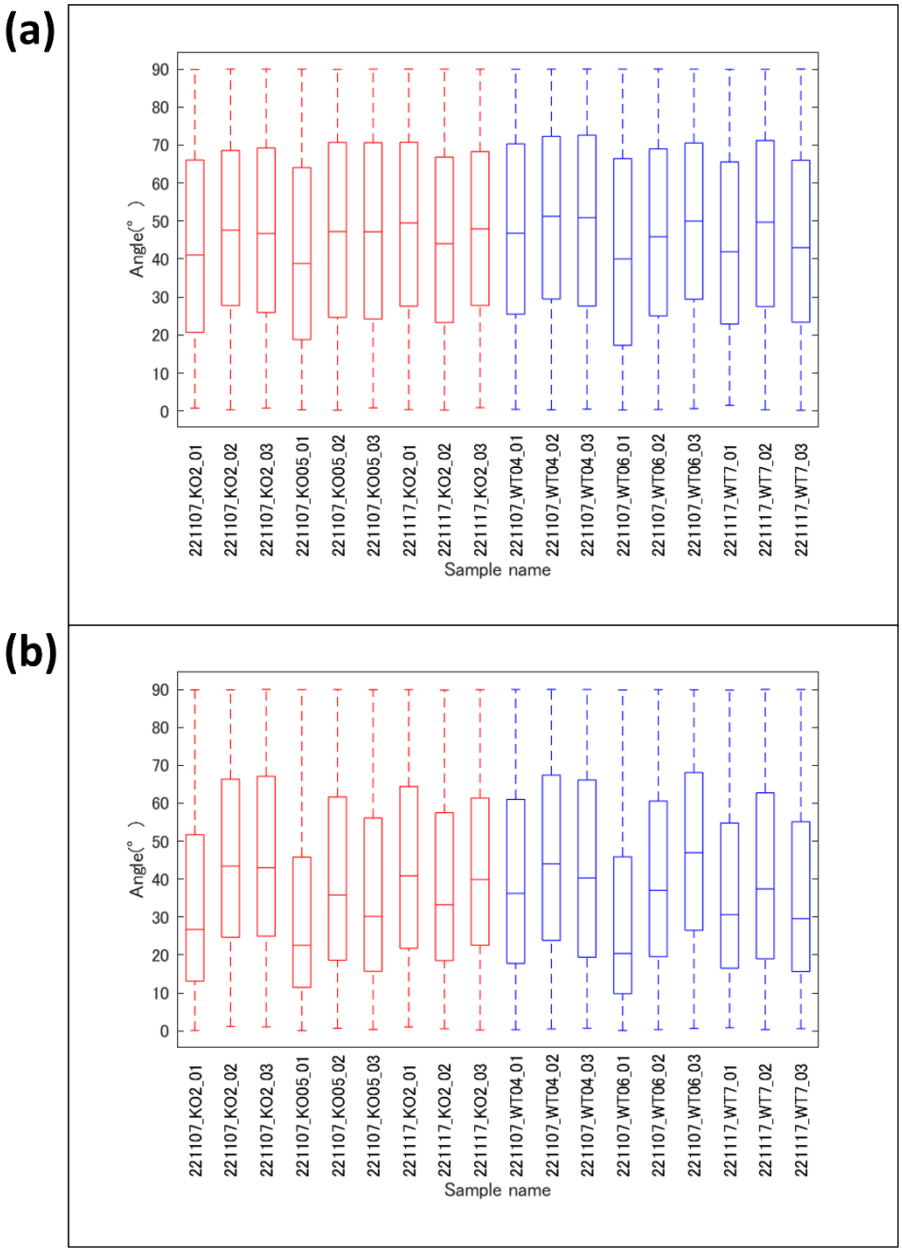

Fig. 8. Angles between myocardial cell nuclei and vascular skeleton. (a) Vascular skeleton length of 50−99 pixels (9.0188−17.8571 microns). (b) Vascular skeleton length exceeding 100 pixels (18.0375 microns).

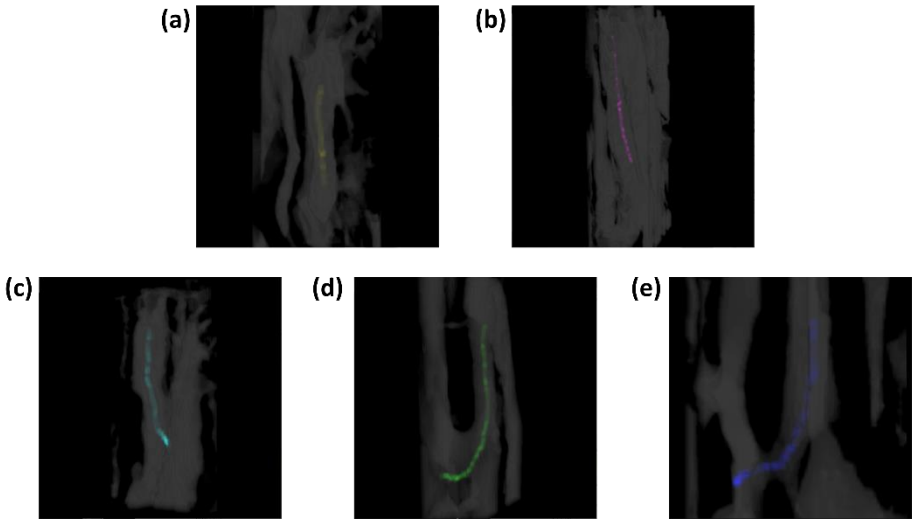

Fig. 9. Examples of straightness visualization. (a) $0.9 \leq s \leq 1.0$. (b) $0.8 \leq s < 0.9$. (c) $0.7 \leq s < 0.8$. (d) $0.6 \leq s < 0.7$. (e) $0.5 \leq s < 0.6$.

5 Conclusion

In this study, we performed a three-dimensional analysis of cellular tissue images of the mouse myocardium, considering the positional relationship between cells and blood vessels. We proposed ‘straightness of blood vessels’ and ‘angle between myocardial cell nucleus and vascular skeleton’ as indices for quantitative evaluation of vascular structure and the relationship between myocardial cells and blood vessels. The results confirmed that differences were observed between WT and KO mice.

In future studies, it will be necessary to conduct a statistical analysis to determine whether significant differences exists between WT and KO mice. In addition, we intend to analyse indices that can be used to quantitatively evaluate the thickness and surface structure of blood vessels and compare them between WT and KO mice. Furthermore, we hope to discriminate between healthy mice and mice with heart defects based on these indices.

References

1. Ministry of Health, Labour and Welfare, Summary of the 2020 Vital Statistics Monthly Report Annual Total (Approximate), https://www.mhlw.go.jp/toukei/saikin/hw/jinkou/geppo/nengai20/dl/gaikyouR2.pdf, last accessed 2023/01/23.
2. Ministry of Education, Culture, Sports, Science and Technology (MEXT) Strategic Research on Heart Failure Elucidation of the Pathogenesis of Heart Failure Using Developmental Engineering and Gene and Cell Therapy, https://www.mext.go.jp/a_menu/shinkou/hojyo/1300506.htm, last accessed 2023/01/23.

3. Bao N. P., Wataru K., Shalini A. M., Jesung M., James F. A., Kate L. P., David G., Beverly A. R., Rui C., Joseph A. G., Celio X. S., SuWannee T., Eiichiro M., Michael T. K., Paul M. R., Serena Z., Shibani M., David J. C., Ahmed I. M., Mauro G., Peter S. R., Asaithamby A., Ajay M. S., Luke I. S., Hesham A. S.: The Oxygen Rich Postnatal Environment Induces Cardiomyocyte Cell Cycle Arrest Through DNA Damage Response. *Cell*, Vol. 157, No. 3, pp.565-579 (2014).
4. Nomura S., Satoh M., Fujita T. et al.: Cardiomyocyte Gene Programs Encoding Morphological and Functional Signatures in Cardiac Hypertrophy and Failure. *Nature Communication* 9, 4435 (2018). https://doi.org/10.1038/s41467-018-06639-7
5. Kalinin A.A., Allyn-Feuer A., Ade A. et al.: 3D Shape Modeling for Cell Nuclear Morphological Analysis and Classification. *Sci Rep* 8, 13658 (2018). https://doi.org/10.1038/s41598-018-31924-2
6. Perona, P., J. Malik. Scale-Space and Edge Detection Using Anisotropic Diffusion. *IEEE® Transactions on Pattern Analysis and Machine Intelligence*. Vol. 12, No. 7, pp. 629-639 (1990).
7. Gerig, G., O. Kubler, R. Kikinis, and F. A. Jolesz. Nonlinear Anisotropic Filtering of MRI Data. *IEEE Transactions on Medical Imaging*. Vol. 11, No. 2, pp. 221-232 (1992).
8. Otsu, N., A Threshold Selection Method from Gray-Level Histograms. *IEEE Transactions on Systems, Man, and Cybernetics*. Vol. 9, No. 1, pp. 6266 (1979).
9. Bradley, D., G. Roth, Adapting Thresholding Using the Integral Image, *Journal of Graphics Tools*. Vol. 12, No. 2, pp.13-21 (2007).
10. Soille, P., Morphological Image Analysis: Principles and Applications, Springer-Verlag, pp. 173-174 (1999).
11. Lee, T.-C., Kashyap, R. L., Chu, C.-N. Building Skeleton Models via 3-D Medial Surface/Axis Thinning Algorithms. *Computer Vision, Graphics, and Image Processing*, Vol. 56, No. 6, pp. 462-478 (1994).
12. Kerschnitzki, M, Kollmannsberger, P, Burghammer, M. et al. Architecture of the Osteocyte Network Correlates with Bone Material Quality. *Journal of Bone and Mineral Research*, Vol. 28, No. 8, pp.1837-1845 (2013).
13. Haralick, R. M., Shapiro, L. G. Computer and Robot Vision, Vol. 1, Addison-Wesley, 1992.
14. Kong, T. Y. and Rosenfeld, A. Topological Algorithms for Digital Image Processing, Elsevier Science, Inc., 1996.
15. Kaneko, S., Arima, Y., Migita, M., Toda, M. Proposal of a Method to Identify Vascular Endothelial Cells from Images of Mouse Myocardial Tissue. In: Sumi, K., Na, I.S., Kaneko, N. (eds) Frontiers of Computer Vision. IW-FCV 2022. *Communications in Computer and Information Science*, vol 1578. Springer, Cham, 2022. https://doi.org/10.1007/978-3-031-06381-7_12
16. Jolliffe, I. T. Principal Component Analysis. 2nd ed., Springer, 2002.
17. Barber, C. B., Dobkin, D. P., Huhdanpaa, H. T. The Quickhull Algorithm for Convex Hulls, ACM Transactions on Mathematical Software, Vol. 22, No. 4, p. 469-483 (1996).
18. Canny, J. A Computational Approach to Edge Detection, IEEE Transactions on Pattern Analysis and Machine Intelligence, Vol. PAMI-8, No. 6, pp. 679-698 (1986).
19. I don't know how to find the angle formed by two vectors, what kind of calculation method is there. https://jp.mathworks.com/matlabcentral/answers/896337-, accessed on 2023/01/23.
20. Yuichiro Arima - IRCMS - Kumamoto University, https://ircms.kumamoto-u.ac.jp/research/yuichiro_arima/, accessed on 2023/01/23.